Tunable nonreciprocal photon correlations induced by directional quantum squeezing

Cai-Peng Shen, Jia-Qiang Chen, Xue-Feng Pan, Yu-Meng Ren, Xing-Liang Dong, Xin-Lei Hei, Yi-Fan Qiao, and Peng-Bo Li*

Ministry of Education Key Laboratory for Nonequilibrium Synthesis and Modulation of Condensed Matter, Shaanxi Province Key Laboratory of Quantum Information and Quantum Optoelectronic Devices, School of Physics, Xi'an Jiaotong University, Xi'an 710049, China

(Received 7 February 2023; revised 19 May 2023; accepted 8 August 2023; published 17 August 2023)

We investigate nonreciprocal photon correlations in coupled microring resonators with directional quantum squeezing (quantum parametric amplification). We show that the degeneracy of two whispering-gallery modes (WGMs) in a microring resonator are broken by applying parametric amplification to one of the WGMs, which makes tunable chiral photon-qubit coupling and chiral photon hopping between two resonators feasible. Selecting optimal quantum squeezing strength, we predict the appearance of nonreciprocal unconventional photon blockade resulting from the interferences among different photon transition-dissipative paths both analytically and numerically. Moreover, flexible conversion between photon bunching and antibunching can be easily realized in a wide range of parameter regimes by modulating the quantum squeezing field. This work provides an alternative way for tunable nonreciprocal photon coherence manipulations in chiral quantum science and technologies.

DOI: 10.1103/PhysRevA.108.023716

I. INTRODUCTION

Photon correlations are one of the quantum correlations, standing for the effective photon-photon coherence interactions, which are important in fundamental science and have wide applications in quantum technologies, such as quantum communication [1–3], quantum computation [4,5], quantum metrology [6,7], and spectroscopy and microscopy [8,9]. Because flying photons rarely interact with one another, manipulating the strongly photonic correlations between individual photons is a long-term research topic in quantum optics. Effective nonlinearities at the single-photon level are necessary for generating strong correlated photon pairs [10], which can be introduced by strong coupling between the light field and single emitters in high-finesse cavities [11–18] or tight-confinement waveguide [19–28]. Nonlinearities in Kerr resonators [29–32], optomechanical systems [33–37], many-body systems [38–42], and other nonlinear processes like spontaneous four-wave mixing [43–45], etc, are used to induce correlated two photons as well. To quantitatively distinguish distinct correlated photon pairs, the second-order correlation function is usually adopted, which reflects the intensity correlations at two space-time points [46]. Correlated photon pairs are categorized as bunching or antibunching by equal-time second-order correlation functions greater or less than unity. Photon bunching states indicate that two photons are attracted to each other, whereas antibunching states indicate that the photons repel each other.

Photon antibunching is a nonclassical quantum phenomena that obeys sub-Poissonian statistics and is used to identify single-photon sources [47,48]. Strong photon antibunching also refers to photon blockade, which indicates that the excitation of the first photon prevents the injection of the second photon into a cavity, resulting in repulsive photon-photon interactions. According to different physical realization mechanisms, there are two types of photon blockade: conventional photon blockade (CPB) and unconventional photon blockade (UPB). UPB is created by destructive interferences between different photon-driven-dissipative routes [49–61], whereas CPB is caused by large anharmonic energy levels resulting in energy mismatch for the second input photon [29,62–64]. Both CPB and UPB have been demonstrated in experiments [15,65–71]. Recently, CPB or UPB combining with quantum nonreciprocity, known as nonreciprocal photon blockade, has attracted much attention [72–81], which extends the potential applications into chiral quantum information processing [82]. The nonreciprocal photon blockade, where the photon blockade emerges for light input from one direction while photon tunneling (photon bunching) arises from the other direction, is usually studied in the spinning ring resonators [83,84]. The induced Sagnac-Fizeau shifts in spinning ring resonators cause degeneracy breaking for two WGMs, which is regarded as the crucial factor for yielding system nonreciprocity. However, rotating the resonators would inevitably introduce the thermal phonons into the system, and the photon correlations at single quantum level could be impacted, especially for the systems involving mechanical degrees of freedom, such as the nonreciprocal UPB investigated with an optomechanical resonator [73]. Thus, one appealing challenge is how to realize nonreciprocal photon blockage or photon correlations in optical microring resonators without spinning and without mechanical degrees of freedom.

In this work, all-optical nonreciprocal photon correlations in microring resonators are studied without the need for Sagnac-Fizeau shifts produced by spinning the resonator,

*lipengbo@mail.xjtu.edu.cn

where two degenerate WGMs in the resonator are split due to one WGM being squeezed by using directional parametric amplification. Parametric amplification has recently been focused on enhancing the effective coupling strength between various quantum systems [37,85–88]. Directional parametric amplification has been used in microring resonator systems to realize frequency conversion [89,90], obtain photon sources [91], and study optical nonreciprocity [92]. In particular, Ref. [92] considers using nonreciprocity to construct diodes and quasicirculators. In our work, under the optimal conditions, nonreciprocal UPB emerges from interferences among three-photon transition-dissipative routes. The chiral couplings between two different polarized two-level systems (TLSs) and corresponding polarized resonator modes provide photon nonlinear transition paths, which in turn leads to symmetric response of the system to external driving when the directional quantum squeezing is not applied. Furthermore, the interference parameters of degenerate modes split, chiral photon hopping and chiral photon-qubit coupling are tunable by adjusting the directional quantum squeezing, allowing for flexible conversion modulations between photon bunching and antibunching in a wide parameter range. Nonreciprocal photon correlations are thus obtained over broad parameter windows. The research advances the manipulation of correlated photons and the development of a prospective nonreciprocal quantum device in chiral quantum optics.

II. MODEL

Consider two microring resonators, A and B, built of high-quality $\chi^{(2)}$ nonlinear thin-film materials. As illustrated in Fig. 1, the two resonators evanescently interact with each other. Due to the strong coherent laser pump field from port 3, the clockwise (CW) WGM in B, $b_{\circlearrowright}$, is exposed to parametric amplification (directional quantum squeezing) under the two-mode phase matching condition [90,92], while the counterclockwise (CCW) WGM, $b_{\circlearrowleft}$, is decoupled. The evanescent field of the CW mode outside resonator B corresponds to σ_- polarized transverse magnetic (TM) modes and only couples to the TLS t_1 with a σ_--polarized transition, while the evanescent field of the CCW mode outside resonator B corresponds to σ_+ polarized TM modes and only couples to the TLS t_2 with a σ_+-polarized transition [16,93–96]. The interaction strengths between B modes and $t_{1,2}$ are J, which is feasible for Rb atoms [93]. In Fig. 1(a), driving field input from port 1 excites CCW mode $a_{\circlearrowleft}$ in A which couples to $b_{\circlearrowright}$ in B with the hopping rate of g. In this situation, the Hamiltonian of the whole system is expressed as (set $\hbar = 1$)

$$
\begin{aligned}
\hat{H} &= \hat{H}_{\mathrm{F}} + \hat{H}_{\mathrm{I}} + \hat{H}_{\mathrm{D}} + \hat{H}_{\mathrm{P}},\\
\hat{H}_{\mathrm{F}} &= \Delta_1 \hat{a}_{\circlearrowleft}^{\dagger}\hat{a}_{\circlearrowleft} + \Delta_2 \hat{b}_{\circlearrowright}^{\dagger}\hat{b}_{\circlearrowright} + \Delta_0 \hat{\sigma}_1^{+}\hat{\sigma}_1^{-},\\
\hat{H}_{\mathrm{I}} &= g(\hat{a}_{\circlearrowleft}^{\dagger}\hat{b}_{\circlearrowright} + \hat{b}_{\circlearrowright}^{\dagger}\hat{a}_{\circlearrowleft}) + J(\hat{\sigma}_1^{+}\hat{b}_{\circlearrowright} + \hat{\sigma}_1^{-}\hat{b}_{\circlearrowright}^{\dagger}),\\
\hat{H}_{\mathrm{D}} &= \varepsilon(\hat{a}_{\circlearrowleft}^{\dagger}e^{-i\Delta t} + \hat{a}_{\circlearrowleft}e^{i\Delta t}),\\
\hat{H}_{\mathrm{P}} &= \frac{\Omega_p}{2}(\hat{b}_{\circlearrowright}^{\dagger 2} + \hat{b}_{\circlearrowright}^{2}),
\end{aligned}
\tag{1}
$$

where $\hat{H}_{\mathrm{F}}$ is the free Hamiltonian for the resonators and the TLS, while $\hat{H}_{\mathrm{I}}$ is the interaction Hamiltonian. $\hat{a}_{\circlearrowleft}^{\dagger}$ ($\hat{a}_{\circlearrowleft}$) is the creation (annihilation) operator of CCW mode in resonator A, while $\hat{b}_{\circlearrowright}^{\dagger}$ ($\hat{b}_{\circlearrowright}$) is the creation (annihilation) operator of CW mode in resonator B. $\Delta_{1,2} = \omega_{a,b} - \omega_p/2$ are the detunings, and $\omega_{a,b}$ are the frequencies of the resonators (A, B). $\sigma_1^{+} = |e\rangle_1\langle g|$ ($\sigma_1^{-} = |g\rangle_1\langle e|$) is the TLS t_1 transition operator with the energy ω_0. $\Delta_0 = \omega_0 - \omega_p/2$ is t_1 detuning and $\Delta = \omega_{in} - \omega_p/2$ is driving field detuning. The frequency of the input driving field is ω_{in}, and its strength is ε. ω_p denotes the pump frequency with the strength Ω_p that is excited by the external coherent laser field from port 3.

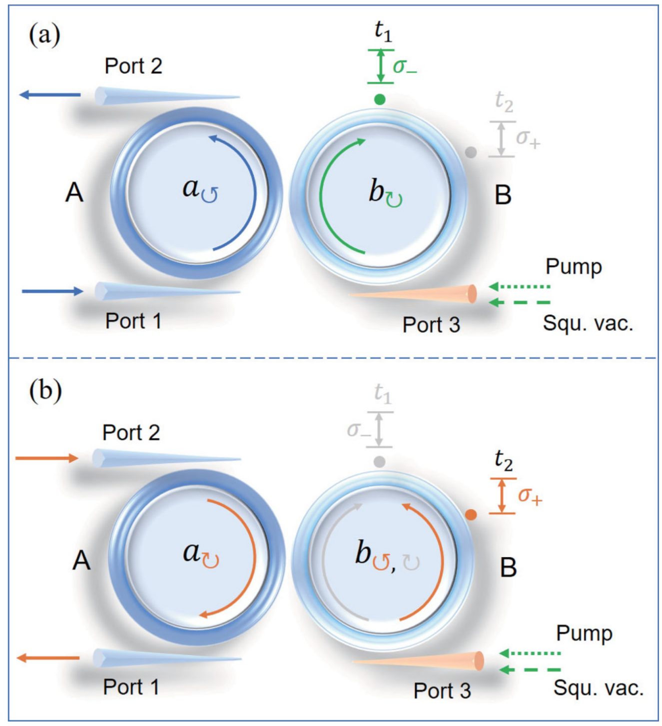

FIG. 1. Diagram of realizing nonreciprocal photon correlations. A strong pump field and a broadband squeezed vacuum field are input from port 3, where the pump field makes CW mode $\hat{b}_{\circlearrowright}$ in resonator B squeezed as $\hat{b}_{\circlearrowright s}$ (directional quantum squeezing), while the squeezed-vacuum field keeps the dissipation of $\hat{b}_{\circlearrowright s}$ the same as that in regular mode. (a) Input driving field from port 1 excites the CCW mode $\hat{a}_{\circlearrowleft}$ in resonator A and interacts with the $\hat{b}_{\circlearrowright s}$ in B. (b) Input driving field from port 2 excites the CW mode $\hat{a}_{\circlearrowright}$ in A and interacts with the CCW mode $\hat{b}_{\circlearrowleft}$ in B.

After executing Bogoliubov transformation $\hat{b}_{\circlearrowright s} = \cosh(r_p)\hat{b}_{\circlearrowright} + \sinh r_p \hat{b}_{\circlearrowright}^{\dagger}$ [37,85], the Hamiltonian in Eq. (1) can be translated into the squeezing picture as

$$
\begin{aligned}
\hat{H}_1 = {}& \Delta_a \hat{a}_1^{\dagger}\hat{a}_1 + \varepsilon(\hat{a}_1^{\dagger} + \hat{a}_1) + \Delta_{bs}\hat{b}_1^{\dagger}\hat{b}_1 + \Delta_t \hat{\sigma}_1^{+}\hat{\sigma}_1^{-}\\
&+ g_1(\hat{a}_1^{\dagger}\hat{b}_1 + \hat{b}_1^{\dagger}\hat{a}_1) + J_1(\hat{\sigma}_1^{+}\hat{b}_1 + \hat{\sigma}_1^{-}\hat{b}_1^{\dagger}),
\end{aligned}
\tag{2}
$$

where $r_p = \ln[(1+\beta)/(1-\beta)]/4$ is the squeezing parameter, while $\beta = \Omega_p/\Delta_2$ is the pump ratio. $\hat{a}_1$ and $\hat{b}_1$ respectively represent $\hat{a}_{\circlearrowleft}$ and $\hat{b}_{\circlearrowright s}$. $\Delta_{a,t} = \omega_{a,0} - \omega_{in} = \Delta_{1,0} - \Delta$ are the effective energies of the resonator A and the TLS t_1, respectively, while $\Delta_{bs} = \Delta_2(1-\beta^2)^{1/2} - \Delta$ is the effective energy of resonator B. $g_1 = g\cosh(r_p)$ [$J_1 = J\cosh(r_p)$] is the effective coupling strength between resonators A and B (t_1 and resonator B). Under the rotating-wave approximation, $g(J)\sinh r_p \ll \Delta_1(\Delta_0) + \Delta_2(1-\beta^2)^{1/2}$, so counter-rotating

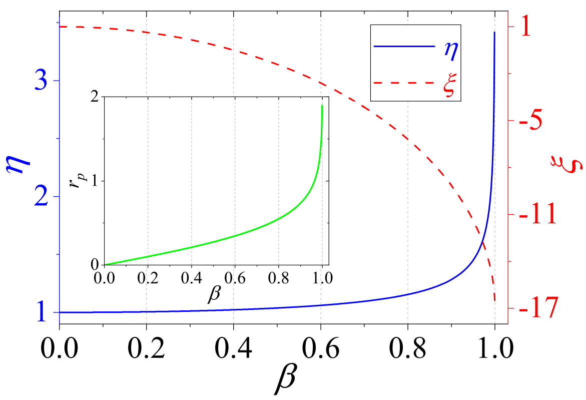

FIG. 2. As a function of pump ratio β, the squeezing parameter r_p (inset figure), chiral coupling ratio η, and mode split ratio ξ are displayed.

terms in Eq. (2), $g\sinh(r_p)\hat{a}_1^\dagger\hat{b}_1^\dagger + J\sinh(r_p)\hat{b}_1^\dagger\sigma_1^+ +$ H.c., are neglected, where H.c. means Hermitian conjugation.

When the driving field inputs through port 2, CW mode $a_\circlearrowright$ in resonator A is excited and couples to $b_\circlearrowright$ in B. $b_\circlearrowright$ is of σ_+ polarization and only couples to the TLS t_2 with a σ_+-polarized transition [93,94]. In this case, the system Hamiltonian reads

$$\hat{H}_2 = \Delta_a\hat{a}_2^\dagger\hat{a}_2 + \varepsilon(\hat{a}_2^\dagger + \hat{a}_2) + \Delta_b\hat{b}_2^\dagger\hat{b}_2 + \Delta_t\hat{\sigma}_2^+\hat{\sigma}_2^- + g_2(\hat{a}_2^\dagger\hat{b}_2 + \hat{b}_2^\dagger\hat{a}_2) + J_2(\hat{\sigma}_2^+\hat{b}_2 + \hat{\sigma}_2^-\hat{b}_2^\dagger), \quad (3)$$

where the effective energy of resonator B is $\Delta_b = \omega_b - \omega_{in} = \Delta_2 - \Delta$. $\hat{a}_2$ and $\hat{b}_2$ respectively represents $\hat{a}_\circlearrowright$ and $\hat{b}_\circlearrowright$. Δ_t is the effective energy of the TLS t_2. Hopping rate between the two resonators is $g_2 = g$ and $J_2 = J$ is the coupling strength between TLS t_2 and resonator B.

It is worth noting that when the directional parametric amplification is not applied, the system chirality introduced by the polarization related chiral couplings of $t_{1,2}$ and B modes plays an important role in eliminating the counter-rotating modes from the interaction, resulting in reciprocal response for external driving fields. Because of the applied directional parametric amplification, the system exhibits nonreciprocal features when the driving field is input from port 1 or port 2. To quantify the difference between these two scenarios, we define the mode split ratio $\xi = \Delta_{bs}/\Delta_b$ and the chiral coupling ratio $\eta = J_1/J_2 = g_1/g_2$. The squeezing parameter (inset figure), chiral coupling ratio, and mode split ratio are displayed against the external pump ratio in Fig. 2. Increasing the pump ratio causes an increase in the squeezing parameter, which indicates a greater squeezed extent for the CW mode in resonator B. The frequency difference between the squeezed CW mode and the CCW mode denotes the degenerate mode split. The mode split ratio ξ, which deviates from 1 as β increases, characterizes the breaking of modes' degeneracy. Similarly, deviation of η from 1 indicates the appearance of system chirality. More squeezing results in a larger mode split extent and higher system chirality. This is the foundation of our work.

As previously discussed, the Bogoliubov transformation transforms photon CW modes in resonator B into squeezing picture, where its effective energy shifts and coupling strength with other systems is enhanced. It is worth noting that the external pump field will inevitably increase the dissipation of CW modes, which could influence our discussions on photon correlations at the single-quantum level. To eliminate this influence, apply the broadband squeezed-vacuum field [37,85] simultaneously from port 3, and the dissipation of squeezed CW modes in resonator B will be unaltered from the normal situation without pump field inputs. Considering the decay of two resonators and TLSs, the evolution of the whole system can be characterized by the master equation

$$\frac{\partial\rho}{\partial t} = -i[\hat{H}_\zeta, \rho] + \kappa_a L[\hat{a}_\zeta]\rho + \kappa_b L[\hat{b}_\zeta]\rho + \gamma L[\hat{\sigma}_\zeta^-]\rho \quad (4)$$

in the Markov and zero-temperature approximations, where $L[\hat{o}]\rho = \hat{o}\rho\hat{o}^\dagger - (\hat{o}^\dagger\hat{o}\rho + \rho\hat{o}^\dagger\hat{o})/2$ is the Lindblad superoperator for operator $\hat{o}$. κ_a (κ_b) is the total decay rate of resonator A (B), while γ is the decay rate of TLSs. $\zeta = 1, 2$ denotes the driving-field inputs from ports 1 and 2, respectively.

III. NONRECIPROCAL PHOTON CORRELATIONS

In this part, we are interested in the output photon correlations from ports 1 and 2 when the driving field is input from distinct ports. The equal-time second-order correlation function $g^{(2)}(0)$ is used to characterize the photon correlations. In the weak driving limit $\varepsilon \ll \kappa_{a,b}, \gamma$, to dominant order, the density operator can be factorized as a pure state and the system is governed by an effective non-Hermitian Hamiltonian [97,98]

$$\hat{\mathcal{H}}_\zeta = \hat{H}_\zeta - i\frac{\kappa_a}{2}\hat{a}_\zeta^\dagger\hat{a}_\zeta - i\frac{\kappa_b}{2}\hat{b}_\zeta^\dagger\hat{b}_\zeta - i\frac{\gamma}{2}\sigma_\zeta^+\sigma_\zeta^-. \quad (5)$$

In weak driving limit, photon correlations can be calculated analytically by truncating the system photon number to two. The wave function of the system is expressed as

$$\begin{aligned}|\psi\rangle_\zeta(t) = {} & C_{0,0,-}^{(\zeta)}|0,0,-\rangle + C_{1,0,-}^{(\zeta)}|1,0,-\rangle \\ & + C_{0,1,-}^{(\zeta)}|0,1,-\rangle + C_{0,0,+}^{(\zeta)}|0,0,+\rangle \\ & + C_{1,1,-}^{(\zeta)}|1,1,-\rangle + C_{1,0,+}^{(\zeta)}|1,0,+\rangle \\ & + C_{0,1,+}^{(\zeta)}|0,1,+\rangle + C_{2,0,-}^{(\zeta)}|2,0,-\rangle \\ & + C_{0,2,-}^{(\zeta)}|0,2,-\rangle, \end{aligned} \quad (6)$$

where $\zeta = 1, 2$ denotes whether the driving field input is from port 1 or port 2. Coefficients $C_{i,j,\pm}^{(\zeta)} = C_{i,j,\pm}^{(\zeta)}(t)$ are the probability amplitudes of the system in states $|i, j, \pm\rangle$. It denotes that there are i photons in resonator A, j photons in resonator B, and the TLS t_ζ in excited (ground) state. In the weak-driving limit, consider different orders of $\varepsilon/(\kappa_{a,b}, \gamma)$; one has [50]

$$\begin{aligned}\left|C_{0,0,-}^{(\zeta)}\right| \gg {} & \left|C_{1,0,-}^{(\zeta)}\right|, \left|C_{0,1,-}^{(\zeta)}\right|, \left|C_{0,0,+}^{(\zeta)}\right| \\ & \gg \left|C_{1,1,-}^{(\zeta)}\right|, \left|C_{1,0,+}^{(\zeta)}\right|, \left|C_{0,1,+}^{(\zeta)}\right|, \left|C_{2,0,-}^{(\zeta)}\right|, \left|C_{0,2,-}^{(\zeta)}\right|. \end{aligned} \quad (7)$$

The system steady state can be obtained by solving $\partial|\psi\rangle_\zeta/\partial_t = 0$ in Schrödinger equation $i\partial|\psi\rangle_\zeta/\partial_t = \hat{\mathcal{H}}_\zeta|\psi\rangle_\zeta$ (see Appendix for calculation details). When the input weak driving field is from port 1 ($\zeta = 1$), the single excitation coefficients are obtained as

$$
\begin{aligned}
C_{0,0,+}^{(1)} &= \frac{\varepsilon J_1 g_1}{\Lambda},\\
C_{0,1,-}^{(1)} &= -\frac{\varepsilon \bar{\Delta}_t g_1}{\Lambda},\\
C_{1,0,-}^{(1)} &= \frac{\varepsilon\left(\bar{\Delta}_{bs}\bar{\Delta}_t - J_1^2\right)}{\Lambda},
\end{aligned}
\tag{8}
$$

where $\Lambda = \bar{\Delta}_t(g_1^2 - \bar{\Delta}_a\bar{\Delta}_{bs}) + \bar{\Delta}_a J_1^2$, $\bar{\Delta}_t = \Delta_t - i\gamma/2$, $\bar{\Delta}_a = \Delta_a - i\kappa_a/2$, $\bar{\Delta}_{bs} = \Delta_{bs} - i\kappa_b/2$. The coefficients of two excitations are not presented here since they are complicated. For the sake of simplicity, it is set to $\omega_a = \omega_b$, $\kappa_a = \kappa_b = \gamma$ hereafter.

According to input-output relations [99], one has $\hat{a}_{1,\text{in}} = \varepsilon/\sqrt{\gamma}$ while $\hat{a}_{2,\text{out}} = \hat{a}_1\sqrt{\gamma}$. When the input photons are from port 1, the equal-time second-order correlation function for the output photons from port 2 is

$$
g_1^{(2)}(0) = \frac{\langle \hat{a}_{2,\text{out}}^{\dagger 2}\hat{a}_{2,\text{out}}^2\rangle}{\langle \hat{a}_{2,\text{out}}^{\dagger}\hat{a}_{2,\text{out}}\rangle^2} = \frac{\langle \hat{a}_1^{\dagger 2}\hat{a}_1^2\rangle}{\langle \hat{a}_1^{\dagger}\hat{a}_1\rangle^2} \approx \frac{2\left|C_{2,0,-}^{(1)}\right|^2}{\left|C_{1,0,-}^{(1)}\right|^4}. \tag{9}
$$

Analytical photon correlations are derived by substituting steady coefficient solutions into $g_1^{(2)}(0)$. Similarly, the equal-time second-order correlation function for photons exiting port 1 can be determined. The correlation functions for the two situations can be presented as

$$
g_\zeta^{(2)}(0) = \frac{\langle \hat{a}_\zeta^{\dagger 2}\hat{a}_\zeta^2\rangle}{\langle \hat{a}_\zeta^{\dagger}\hat{a}_\zeta\rangle^2} \approx \frac{2\left|C_{2,0,-}^{(\zeta)}\right|^2}{\left|C_{1,0,-}^{(\zeta)}\right|^4}. \tag{10}
$$

Photon bunching or antibunching is denoted by $g_\zeta^{(2)}(0) > 1$ or $g_\zeta^{(2)}(0) < 1$. The mean photon number of the system is much smaller than one for weak input driving fields, and photon antibunching also represents for photon blockade [72], i.e., nonclassical photon sub-Poissonian distributions. UPB occurs if $|C_{2,0,-}^{(\zeta)}| = 0$ is satisfied, which makes $g_\zeta^{(2)}(0) \to 0$. UPB is caused by the interference of distinct photon transition paths. Specifically, the interference is caused by three photon driven paths: (a) direct driven excitation, $|1,0,-\rangle \xrightarrow{\sqrt{2}\varepsilon} |2,0,-\rangle$; (b) indirect driven transition, $|1,0,-\rangle \xrightarrow{g_\zeta} |0,1,-\rangle \xrightarrow{\varepsilon} |1,1,-\rangle \xrightarrow{\sqrt{2}g_\zeta} |2,0,-\rangle$; (c) indirect driven transition, $|1,0,-\rangle \xrightarrow{g_\zeta} |0,1,-\rangle \xrightarrow{J_\zeta} |0,0,+\rangle \xrightarrow{\varepsilon} |1,0,+\rangle \xrightarrow{J_\zeta} |1,1,-\rangle \xrightarrow{\sqrt{2}g_\zeta} |2,0,-\rangle$. In the presence of proper parameters, destructive interference among these transition paths would result in little population on $C_{2,0,-}^{(\zeta)}$ and guarantee the appearance of UPB.

Based on Eqs. (10) and (4), one can explore the equal-time second-order photon correlation functions analytically and numerically. Equal-time second-order correlation functions on a logarithmic scale are displayed in Fig. 3 as a function of pump ratio. It shows that $g_2^{(2)}(0)$ is unaffected by the pump ratio due to decoupling, whereas $g_1^{(2)}(0)$ decreases from a value greater than 1 to that less than 1 with increasing the pump ratio and reaches its lowest value at $\beta \simeq 0.102$. The analytical findings correspond well with the numerical results. As the pump ratio increases, the effective frequency of the squeezed

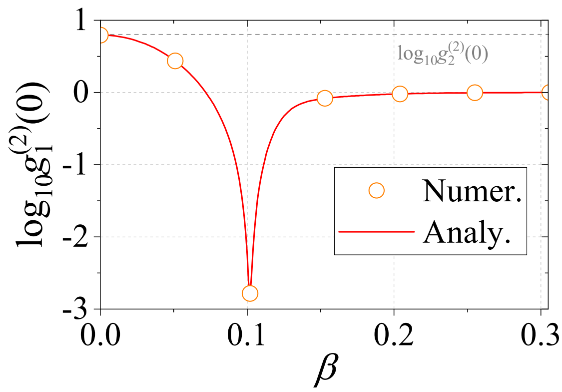

FIG. 3. The logarithmic scaled equal-time second-order functions are shown by altering the pump ratio β. The horizontal dark gray dashed line represents $\log_{10} g_2^{(2)}(0)$. The parameters are set to $J = 2\gamma$, $g = 3.2\gamma$, $\Delta = 1\times 10^2 g$, and $\Delta_1 = \Delta_2 = \Delta_0 = \Delta + \gamma$.

CW mode $\Delta_{bs} = \Delta_2(1-\beta^2)^{1/2} - \Delta$ in resonator B drops, resulting in an increasing detuning between the squeezed CW mode and the TLS t_1 frequencies. A larger detuning of the photon-TLS interaction means a gradually invalid nonlinear response, i.e., the system nonlinearity is destroyed, and it leads to the disappearance of photon correlations. Subsequently, the appearance of $\log_{10} g_1^{(2)}(0) \to 0$ does so for this reason.

Analytical calculations with a set of parameters, $\Delta_a = \Delta_b = \Delta_t = \gamma$, $g = 3.2\gamma$, and $\Delta = 1\times 10^2 g$, reveal that $J \simeq 2\gamma$ and $\beta \simeq 0.102$ are required to yield $C_{2,0,-}^{(1)}$ and $g_1^{(2)}(0) \to 0$, which is the optimal UPB condition. At the same time, these specific parameters also lead to $g_2^{(2)}(0) > 1$. It indicates that nonreciprocal photon blockade is obtained, i.e., the photons produced by various ports exhibit opposing correlation features.

In Figs. 4(a) and 4(b), $\log_{10} g_\zeta^{(2)}(0)$ is shown as the functions of photon-qubit interaction strength J and photon hopping rate g, respectively, where the legends, *i-j, numer./analy.*, stand for the numerical/analytical results for photons input from port i and output from port j. Except for the dips around about $g \simeq 3.2\gamma$ and $J \simeq 2\gamma$, it can be observed that the analytical results and the numerical results are in good agreement. The distinct truncated photon number space is what causes discrepancies between the analytical and numerical conclusions around the dips. As has been mentioned above, analytical calculations truncate the photon number to two. Numerical computations are restricted to three photons. The second-order correlation functions at about the optimal UPB parameters are somewhat affected by higher photon number excitations, which causes the analytical results to be a bit bigger than the numerical values. In Fig. 4(a), when fixing $g = 3.2\gamma$, a parameter window of nonreciprocal (opposite) photon correlations arises during $0.5\gamma \lesssim J \lesssim 3.3\gamma$, which is marked by the shaded area SA 1. The parameter window of nonreciprocal photon correlations also appears during $0.5\gamma \lesssim g \leqslant 10\gamma$ when fixing $J = 2\gamma$ in Fig. 4(b).

According to the preceding discussions, nonreciprocal photon correlations exist over a wide range of parameter g and also over a narrower parameter window of J. In Fig. 5, $g_\zeta^{(2)}(0)$ is further shown as a function of g and J. A contour

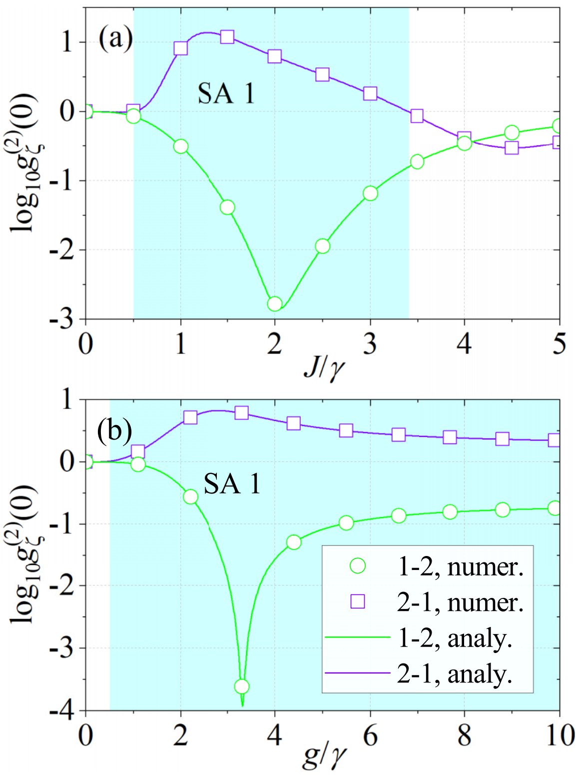

FIG. 4. Equal-time second-order correlation functions $\log_{10} g_\zeta^{(2)}(0)$ are displayed as functions with the parameters (a) J and (b) g. The driving field input from port i and output from port j are referred to as i-j. Numerical results are marked by a green circle and a violet square, while analytical results are marked by green and violet lines. The parameter window within which nonreciprocal (opposite) photon correlations arise is shown by the shaded region marked by SA 1. It is set to $\varepsilon = 0.02\gamma$, $\beta = 0.102$ and other parameters are same with that in Fig. 3.

line of $\log_{10} g_\zeta^{(2)}(0) \simeq 0$ is added in the figures. Figure 5(a) shows that photons output from port 2 nearly totally display antibunching across the parameter space. When photons are output from port 1 in Fig. 5(b), photon bunching is seen across a wide range of g for the value of $J \lesssim 3\gamma$. The efficient region for obtaining nonreciprocal photon correlations is indicated

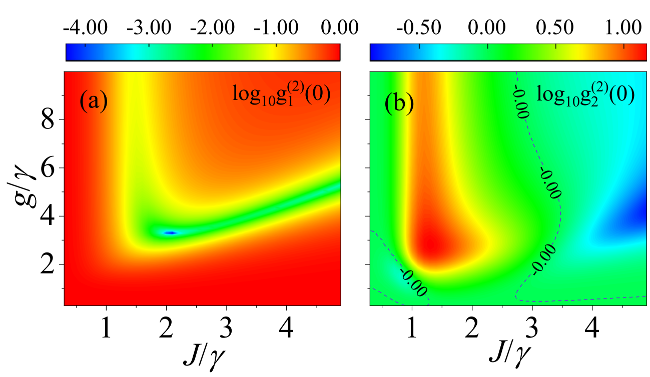

FIG. 5. The results of $\log_{10} g_{1,2}^{(2)}(0)$ against g and J are shown in [(a),(b)]. The violet dashed line is the contour of $\log_{10} g_{1,2}^{(2)}(0) \simeq 0.00$. The other parameters are same with that in Fig. 4.

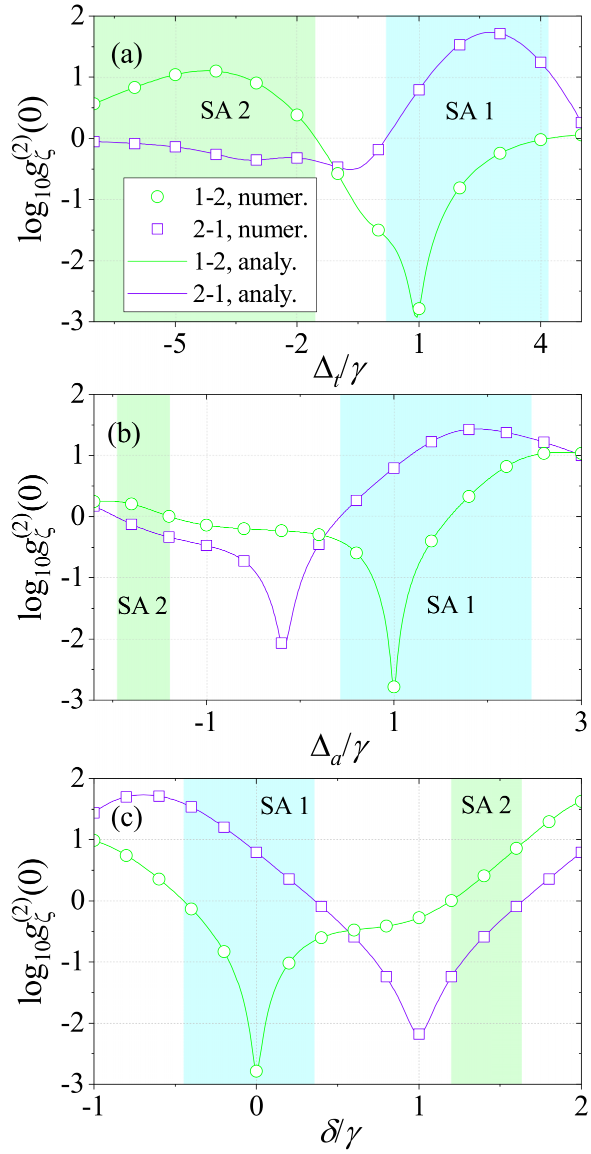

FIG. 6. Plots of the equal-time second-order functions versus the effective frequencies of the TLS, resonator, and driving field are shown in panels [(a)–(c)], respectively. The shaded areas labeled SA 1 and SA 2 are two distinct parameter windows of nonreciprocal photon correlations. The other parameters are same with that in Fig. 4.

by the parameter space where different photon correlations occur ($\zeta = 1, 2$). It is evident that, in contrast to the photon-qubit interaction strength J, nonreciprocal photon correlations are less susceptible to the effects of photon hopping rate g. This can be explained by the fact that the photon correlations are more significantly affected by the nonlinearity induced by the photon-qubit interaction, and the nonlinear response significantly influences the photon interference.

Functions of $g_\zeta^{(2)}(0)$ versus the effective TLS frequency Δ_t, the effective resonator frequency Δ_a ($\Delta_a = \Delta_b$), and the effective driving field frequency δ ($\delta = \Delta - 10^2 g$) are depicted in Figs. 6(a)–6(c), respectively, to examine the nonreciprocal photon correlations in various parameter spaces. The analytical results match the numerical results well. Photons from port 2 display antibunching behavior while photons from port 1 display bunching behavior within the parameter window SA 1. Contrarily, in the parameter window denoted by shaded region SA 2, there exist opposing nonreciprocal photon correlations, with photons output from port 1 behaving in an antibunching state while behaving in a bunching state from port 2. Varied photon interferences during the distinct disconnected parameter windows are the root cause of the two types of nonreciprocal photon correlations. As previously stated, nonreciprocal UPB are caused by the specific parameter condition. This gives us the idea to see if the adjustable system chirality by modulating external pump field can make it possible for nonreciprocal photon correlations in a wide range of consecutive parameters. In other words, photons output at distinct ports always exhibit different correlations with one another in widen parameter windows. The next part will be devoted to this subject.

IV. TUNABILITY OF NONRECIPROCAL PHOTON CORRELATIONS

Nonreciprocal photon correlations have been examined in the last section in regard to various parameter spaces under a fixed directional squeezing parameter. The nonreciprocal photon correlations are contributed during distinct and disconnected frequency parameter windows (SA 1, SA 2). In this section, we will research ways to expand the frequency parameter spaces for nonreciprocal photon correlations by tuning the squeezing pump field.

Two types of parameter windows (SA 1, SA 2) are illustrated for realizing nonreciprocal photon correlations in Fig. 6. However, the parameter windows regarding the effective frequencies of TLS, resonator, and input driving field appear to be narrow, thus we hope to broaden the parameter windows to boost the research practicality. Figure 3 has shown the tunability of nonreciprocal photon correlations by modifying the pump ratio, which is promising for use in broadening the valuable parameter spaces for nonreciprocal photon correlations. At the optimal UPB condition, $\log_{10} g_1^{(2)}(0)$ is displayed against the effective frequencies of TLS, resonator, and the input driving field for varied pump ratio β in Figs. 7(a), 7(b); 7(c), 7(d); and 7(e), 7(f), respectively. Figures 7(a), 7(c), 7(e) and 7(b), 7(d), 7(f) depict the equal-time second-order correlation function in logarithmic scale within intervals $\leqslant -0.05$ and $\geqslant 0.05$, respectively. It is observed that one can always find a β to make $\log_{10} g_1^{(2)}(0) \leqslant -0.05$ when the TLS effective frequency $\Delta_t \in [-10, 10]\gamma$. Additionally, we can nearly always locate a β to make $\log_{10} g_1^{(2)}(0) \geqslant 0.05$ during $\Delta_t \in [-10, 10]\gamma$. Regarding the effective frequency $\Delta_a \in [0, 16]\gamma$ or $\delta \in [-6, 2]\gamma$, $\log_{10} g_1^{(2)}(0) \leqslant -0.05$ is always achieved for one suitable β. Similarly, a β can almost always be found to make $\log_{10} g_1^{(2)}(0) \geqslant 0.05$ for $\Delta_a \in [0, 16]\gamma$ or $\delta \in [-6, 2]\gamma$. The findings indicate a widening of the parameter space for nonreciprocal photon correlations. In particular, for any parameter in these large parameter spaces, photon antibunching state is always acquired at port 2 when the photons output from port 1 exhibit bunching state. While for the majority of regions in the widening parameter spaces, photon bunching state is always achieved at port 2, if the photons output from port 1 show antibunching state. In brief, photon correlations produced from port 2 can be either antibunching states or bunching states in a wide parameter range by altering the external pump field. The changeability of the split resonator modes, chiral photon hopping rate, and chiral photon-TLS coupling rate are the main causes of the variable interferences among the photon transition paths, which give rise to the tunable nonreciprocal photon correlations. Thus, these movable parameters allow the photon correlations to be modified from optimal UPB to that with photon super-Poissonian distributions.

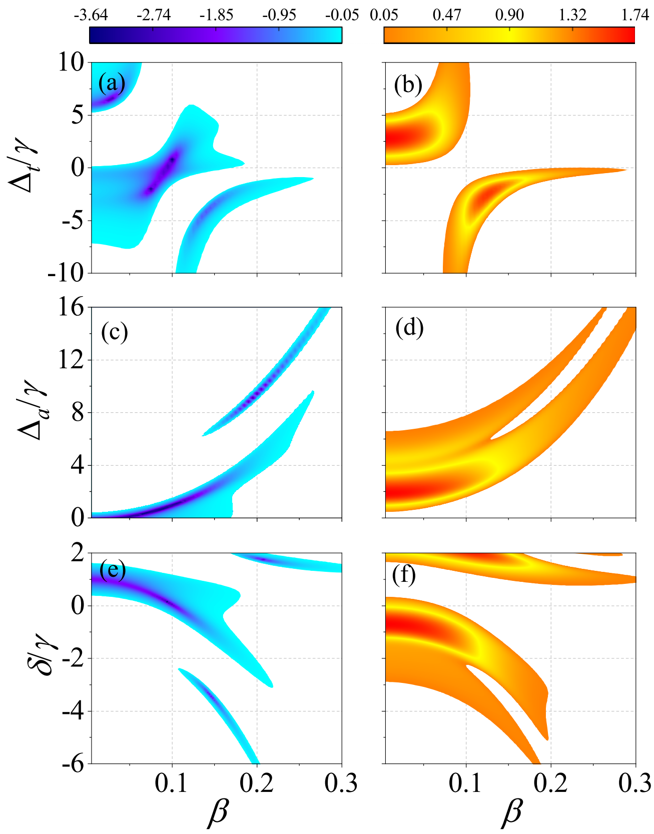

FIG. 7. For different pump ratio, $\log_{10} g_1^{(2)}(0)$ is shown in panels (a), (b); (c), (d); and (e), (f), respectively, against the effective frequencies of TLS, resonator, and input driving field. Panels (a), (c), and (e) show results in the interval $\leqslant -0.05$, whereas panels (b), (d), and (f) show results in the interval $\geqslant 0.05$. The other parameters are the same as those in Fig. 4.

V. EXPERIMENTAL FEASIBILITY

Thin-film materials like lithium niobate [100–102], aluminum nitride [89,90], or silicon nitride [103] can be used to create microring resonators with large $\chi^{(2)}$ nonlinearity due to their advancements in experimental fabrication. Since the ultrahigh quality of lithium niobate microring resonators have been experimentally increased from 10^7 [104] to above 10^8 [105], they are better appropriate for our investigation. An ultrabright photon pair has been observed in an experiment exploiting the large second-order nonlinearity in a lithium niobate microring resonator [91]. When $Q \simeq 6.7 \times 10^7$, the decay rate of a resonator with a given wavelength of $\lambda \simeq 1550$ nm

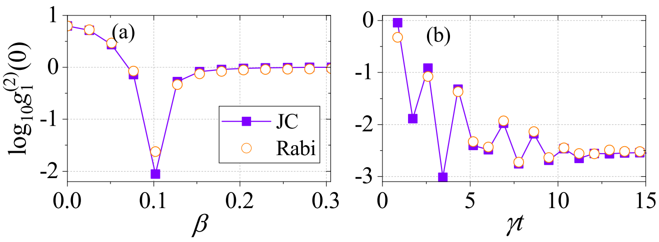

FIG. 8. (a) The equal-time second-order correlation function $g_1^{(2)}(0)$ versus β is plotted for the JC model and the Rabi model. (b) Evolution of $g_1^{(2)}(t)$ versus time t at the corresponding optimal UPB condition when detuning $\Delta = 1 \times 10^3\gamma$. The other parameters are the same as those in Fig. 4.

is $\kappa_{a,b} \simeq 2\pi \times 3\,\mathrm{MHz}$. The strength of photon evanescent hopping g depends on the size of the gap between the microring resonators. The gap size of the tapered fibers and resonators can also be used to modify their evanescent coupling J [106–108]. Broadband squeezed-vacuum fields have been reported in experiments via optical parametric amplification [109] and spontaneous four-wave mixing [110]. Strong chiral coupling of a polarized TLS with a microring resonator has been observed in experiments with a decay rate of $\gamma \simeq \kappa_{a,b}$ [16,93,94].

The counter-rotating terms in Eq. (2) are neglected after considering the rotating-wave approximation in Bogoliubov transformations. To demonstrate the approximation validity, in Fig. 8(a), we compare the photon correlation results under the entire Hamiltonian without neglecting counter-rotating terms with the Hamiltonian neglecting counter-rotating terms, i.e., the results from the time-dependent Rabi model and the time-dependent JC model. It is shown that the two results agree well with each other except for the regions around optimal UPB. This is because the optimal UPB strictly depends on the interference of different photon transition paths, and the photon fluctuation (from counter-rotating terms) would influence the photon correlations. To suppress this influence, one can select a larger parameter to better satisfy the rotating-wave approximation. In Fig. 8(b), choosing $\Delta = 1 \times 10^3\gamma$ and keeping parameters $\Delta_a = \Delta_b = \Delta_t = \gamma$ and g, J unchanged, the evolutions of $g_1^{(2)}(t)$ versus time t for the Rabi model and the JC model are respectively plotted at the corresponding optimal UPB condition ($\beta \simeq 0.058$), where the two results ultimately are in good agreement compared with those in Fig. 8(a).

The above results are discussed under the zero-temperature approximation and the effect of thermal bath is not considered. Next, we discuss the effect of the thermal bath on resonators and TLSs. Considering the thermal bath effect, the Lindblad operator $\gamma L[\hat{o}_\zeta]\rho$ in Eq. (4) should be rewritten as $(\bar{n}+1)\gamma L[\hat{o}_\zeta]\rho + \bar{n}\gamma L[\hat{o}_\zeta^\dagger]\rho$, where the thermal excitation numbers $\bar{n} = \bar{n}_a, \bar{n}_b, \bar{n}_t$, respectively, correspond to $\hat{o} = \hat{a}, \hat{b}, \hat{\sigma}^-$. Figures 9(a)–9(c) show the influences of thermal excitations in resonator A ($\bar{n}_a$), resonator B ($\bar{n}_b$), and TLSs ($\bar{n}_t$) on the second-order correlation functions, respectively. It is shown that $g_1^{(2)}$ ($g_2^{(2)}$) increases (decreases) with the increase in thermal excitation numbers. The thermal baths for resonators A and B almost have the same effect on the nonreciprocal photon correlations, while the thermal baths for the TLSs have a smaller influence on the photon correlations. Because the photon correlations in our studies result from the interference among different photon transition paths, the photon fluctuations from the thermal bath would obviously influence the photon transitions. Comparing with other bosons like phonons and magnons, the thermal photon number for optical systems is usually negligible. Thus, the thermal bath might not have a significant impact on the results.

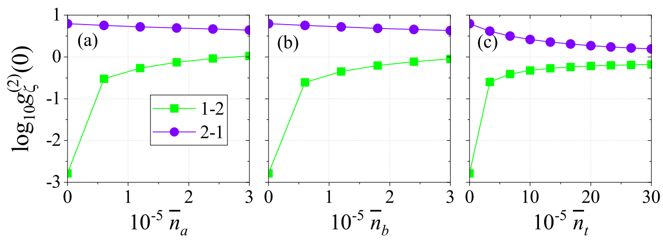

FIG. 9. Equal-time second-order correlation functions $g_\zeta^{(2)}(0)$ are displayed versus the thermal excitation numbers in (a) resonator A, (b) resonator B, and (c) TLSs at the optimal UPB condition. The other parameters are the same as those in Fig. 4.

VI. SUMMARY

Nonreciprocal photon correlations are studied in microring resonators coupled with polarized TLSs by introducing directional parametric amplification. Both the mechanical degree of freedom and Sagnac-Fizeau shifts by rotating microring resonators are not required. Degenerate resonator modes splitting, chiral photon-TLS coupling, and chiral photon hopping are tunable by adjusting the directional parametric amplification. According to analytical and numerical results, under the optimal conditions, interferences among various photon transition-dissipative routes result in nonreciprocal UPB. Additionally, the external pump field is used to adjust the photon correlations and further extend the parameter windows for nonreciprocal photon correlations. As a result, the nonreciprocal photon correlations are robust to parameter fluctuations and are feasible across a wide range of parameters. Our research provides a promising nonreciprocal single-quantum device for manipulating correlated photons and can be exploited to investigate other quantum phenomena like nonreciprocal coherent polariton dynamics [111] or nonreciprocal time crystalline phases [112].

ACKNOWLEDGMENTS

This work is supported by the National Natural Science Foundation of China under Grant No. 92065105, and the Natural Science Basic Research Program of Shaanxi (Program No. 2020JC-02). The Qutip library in Python [113] is used for numerical simulations.

APPENDIX: CALCULATIONS OF EQUAL-TIME SECOND-ORDER CORRELATION FUNCTIONS

In the main text, it is shown that equal-time second-order correlation functions $g_\zeta^{(2)}(0)$ can be calculated analytically by substituting $C_{2,0,-}^{(\zeta)}$ and $C_{1,0,-}^{(\zeta)}$ into Eq. (10). Next, we mainly focus on the detailed calculations for solving $g_1^{(2)}(0)$ when driving field is input from port 1, and similar calculations can be used to determine the solutions for $g_2^{(2)}(0)$. To obtain the system steady solutions, one needs to solve $\partial|\psi\rangle_1/\partial_t = 0$ by substituting the wave function $|\psi\rangle_1$ in Eq. (6) and the system Hamiltonian in Eq. (5) into the Schrödinger equation $i\partial|\psi\rangle_1/\partial_t = \hat{\mathcal{H}}_1|\psi\rangle_1$. Then we have the functions

$$\begin{aligned}
0 &= \bar{\Delta}_a C_{1,0,-}^{(1)} + g_1 C_{0,1,-}^{(1)} + \varepsilon,\\
0 &= \bar{\Delta}_{bs} C_{0,1,-}^{(1)} + g_1 C_{1,0,-}^{(1)} + J_1 C_{0,0,+}^{(1)},\\
0 &= \bar{\Delta}_t C_{0,0,+}^{(1)} + J_1 C_{0,1,-}^{(1)},\\
0 &= \bar{\Delta}_a C_{1,1,-}^{(1)} + \varepsilon C_{0,1,-}^{(1)} + \bar{\Delta}_{bs} C_{1,1,-}^{(1)} + J_1 C_{1,0,+}^{(1)}\\
&\quad + \sqrt{2} g_1 \big(C_{0,2,-}^{(1)} + C_{2,0,-}^{(1)}\big),\\
0 &= \bar{\Delta}_a C_{1,0,+}^{(1)} + \varepsilon C_{0,0,+}^{(1)} + \bar{\Delta}_t C_{1,0,+}^{(1)}\\
&\quad + g_1 C_{0,1,+}^{(1)} + J_1 C_{1,1,-}^{(1)},\\
0 &= \bar{\Delta}_{bs} C_{0,1,+}^{(1)} + g_1 C_{1,0,+}^{(1)} + \sqrt{2} J_1 C_{0,2,-}^{(1)} + \bar{\Delta}_t C_{0,1,+}^{(1)},\\
0 &= \sqrt{2}\bar{\Delta}_a C_{2,0,-}^{(1)} + \varepsilon C_{1,0,-}^{(1)} + g_1 C_{1,1,-}^{(1)},\\
0 &= \sqrt{2}\bar{\Delta}_{bs} C_{0,2,-}^{(1)} + g_1 C_{1,1,-}^{(1)} + J_1 C_{0,1,+}^{(1)},
\end{aligned} \tag{A1}$$

where $C_{0,0,-}^{(1)}$ is assumed to be $\to 1$ due to the weak driving limit, and $\bar{\Delta}_a = \Delta_a - i\kappa_a/2$, $\bar{\Delta}_{bs} = \Delta_{bs} - i\kappa_b/2$, $\bar{\Delta}_t = \Delta_t - i\gamma/2$. The single excitation solutions are obtained as

$$\begin{aligned}
C_{0,0,+}^{(1)} &= \frac{\varepsilon J_1 g_1}{\Lambda},\\
C_{0,1,-}^{(1)} &= -\frac{\varepsilon \bar{\Delta}_t g_1}{\Lambda},\\
C_{1,0,-}^{(1)} &= \frac{\varepsilon\big(\bar{\Delta}_{bs}\bar{\Delta}_t - J_1^2\big)}{\Lambda},
\end{aligned} \tag{A2}$$

after solving the first three functions in Eq. (A1), where $\Lambda = \bar{\Delta}_t(g_1^2 - \bar{\Delta}_a\bar{\Delta}_{bs}) + \bar{\Delta}_a J_1^2$. Two-excitation solutions can then be solved by substituting these single excitation solutions into the last five functions of Eq. (A1). Since the two-excitation solutions are complex, we only give the expression of coefficient $C_{2,0,-}^{(1)}$ as

$$C_{2,0,-}^{(1)} = -\frac{\varepsilon^2 \Xi}{\sqrt{2}\Lambda\Pi}, \tag{A3}$$

where

$$\begin{aligned}
\Xi &= \bar{\Delta}_{bs}^2\bar{\Delta}_t\chi - J_1^2\big[\bar{\Delta}_a^2\nu + \bar{\Delta}_{bs}^2\big(2\bar{\Delta}_{bs}\bar{\Delta}_t + 3\bar{\Delta}_t^2 - 2g_1^2\big)\\
&\quad + \mu\nu - 2\bar{\Delta}_{bs}\bar{\Delta}_a g_1^2\big] + J_1^4\big(\bar{\Delta}_a^2 + \bar{\Delta}_{bs}^2 + 3\bar{\Delta}_{bs}\bar{\Delta}_t\\
&\quad + \mu + g_1^2\big) - J_1^6,\\
\Pi &= \big(\bar{\Delta}_a\bar{\Delta}_{bs} - g_1^2\big)\chi - J_1^2\big[\bar{\Delta}_a\big(\bar{\Delta}_a^2 + \mu + \nu\big)\\
&\quad + (\bar{\Delta}_a - \bar{\Delta}_t)g_1^2\big] + \bar{\Delta}_a J_1^4,\\
\chi &= (\bar{\Delta}_a + \bar{\Delta}_{bs})\big[(\bar{\Delta}_a + \bar{\Delta}_t)(\bar{\Delta}_{bs} + \bar{\Delta}_t) - g_1^2\big],\\
\nu &= \bar{\Delta}_{bs}(\bar{\Delta}_{bs} + 2\bar{\Delta}_t),\\
\mu &= \bar{\Delta}_a(\bar{\Delta}_{bs} + \bar{\Delta}_t).
\end{aligned}$$

With the solved coefficients $C_{2,0,-}^{(1)}$ and $C_{1,0,-}^{(1)}$, the equal-time second-order correlation function for photons output from port 2 can be analytically obtained by Eq. (9) as

$$g_1^{(2)}(0) = \frac{|\Xi|^2|\Lambda|^2}{|\Pi|^2\big|\bar{\Delta}_{bs}\bar{\Delta}_t - J_1^2\big|^4}. \tag{A4}$$

Additionally, by setting β to zero, the $g_2^{(2)}(0)$ for photons produced from port 1 can be analytically solved using the same procedures.

[1] H. J. Kimble, The quantum internet, Nature (London) **453**, 1023 (2008).
[2] J. L. O'brien, A. Furusawa, and J. Vučković, Photonic quantum technologies, Nat. Photon. **3**, 687 (2009).
[3] A. Reiserer and G. Rempe, Cavity-based quantum networks with single atoms and optical photons, Rev. Mod. Phys. **87**, 1379 (2015).
[4] P. Walther, K. J. Resch, T. Rudolph, E. Schenck, H. Weinfurter, V. Vedral, M. Aspelmeyer, and A. Zeilinger, Experimental one-way quantum computing, Nature (London) **434**, 169 (2005).
[5] P. Kok, W. J. Munro, K. Nemoto, T. C. Ralph, J. P. Dowling, and G. J. Milburn, Linear optical quantum computing with photonic qubits, Rev. Mod. Phys. **79**, 135 (2007).
[6] V. Giovannetti, S. Lloyd, and L. Maccone, Advances in quantum metrology, Nat. Photon. **5**, 222 (2011).
[7] D. Braun, G. Adesso, F. Benatti, R. Floreanini, U. Marzolino, M. W. Mitchell, and S. Pirandola, Quantum-enhanced measurements without entanglement, Rev. Mod. Phys. **90**, 035006 (2018).
[8] K. E. Dorfman, F. Schlawin, and S. Mukamel, Nonlinear optical signals and spectroscopy with quantum light, Rev. Mod. Phys. **88**, 045008 (2016).
[9] G. Lubin, D. Oron, U. Rossman, R. Tenne, and V. J. Yallapragada, Photon correlations in spectroscopy and microscopy, ACS Photon. **9**, 2891 (2022).
[10] D. E. Chang, V. Vuletić, and M. D. Lukin, Quantum nonlinear optics-photon by photon, Nat. Photon. **8**, 685 (2014).
[11] J. M. Raimond, M. Brune, and S. Haroche, Manipulating quantum entanglement with atoms and photons in a cavity, Rev. Mod. Phys. **73**, 565 (2001).
[12] H. Mabuchi and A. Doherty, Cavity quantum electrodynamics: Coherence in context, Science **298**, 1372 (2002).
[13] K. Hennessy, A. Badolato, M. Winger, D. Gerace, M. Atatüre, S. Gulde, S. Fält, E. L. Hu, and A. Imamoğlu, Quantum nature of a strongly coupled single quantum dot–cavity system, Nature (London) **445**, 896 (2007).
[14] A. Kubanek, A. Ourjoumtsev, I. Schuster, M. Koch, P. W. H. Pinkse, K. Murr, and G. Rempe, Two-Photon Gateway in One-Atom Cavity Quantum Electrodynamics, Phys. Rev. Lett. **101**, 203602 (2008).
[15] A. Reinhard, T. Volz, M. Winger, A. Badolato, K. J. Hennessy, E. L. Hu, and A. Imamoğlu, Strongly correlated photons on a chip, Nat. Photon. **6**, 93 (2012).
[16] I. Shomroni, S. Rosenblum, Y. Lovsky, O. Bechler, G. Guendelman, and B. Dayan, All-optical routing of single

photons by a one-atom switch controlled by a single photon, Science **345**, 903 (2014).
[17] B. Hacker, S. Welte, G. Rempe, and S. Ritter, A photon–photon quantum gate based on a single atom in an optical resonator, Nature (London) **536**, 193 (2016).
[18] C. S. Munoz, F. P. Laussy, E. del Valle, C. Tejedor, and A. González-Tudela, Filtering multiphoton emission from state-of-the-art cavity quantum electrodynamics, Optica **5**, 14 (2018).
[19] J.-T. Shen and S. Fan, Strongly Correlated Two-Photon Transport in a One-Dimensional Waveguide Coupled to a Two-Level System, Phys. Rev. Lett. **98**, 153003 (2007).
[20] J.-T. Shen and S. Fan, Strongly correlated multiparticle transport in one dimension through a quantum impurity, Phys. Rev. A **76**, 062709 (2007).
[21] D. Roy, Two-Photon Scattering by a Driven Three-Level Emitter in a One-Dimensional Waveguide and Electromagnetically Induced Transparency, Phys. Rev. Lett. **106**, 053601 (2011).
[22] P. Kolchin, R. F. Oulton, and X. Zhang, Nonlinear Quantum Optics in a Waveguide: Distinct Single Photons Strongly Interacting at the Single Atom Level, Phys. Rev. Lett. **106**, 113601 (2011).
[23] H. Zheng, D. J. Gauthier, and H. U. Baranger, Cavity-Free Photon Blockade Induced by Many-Body Bound States, Phys. Rev. Lett. **107**, 223601 (2011).
[24] S. Faez, P. Türschmann, H. R. Haakh, S. Götzinger, and V. Sandoghdar, Coherent Interaction of Light and Single Molecules in a Dielectric Nanoguide, Phys. Rev. Lett. **113**, 213601 (2014).
[25] Y. Shen and J.-T. Shen, Photonic-Fock-state scattering in a waveguide-QED system and their correlation functions, Phys. Rev. A **92**, 033803 (2015).
[26] P. Lodahl, S. Mahmoodian, and S. Stobbe, Interfacing single photons and single quantum dots with photonic nanostructures, Rev. Mod. Phys. **87**, 347 (2015).
[27] A. Sipahigil, R. E. Evans, D. D. Sukachev, M. J. Burek, J. Borregaard, M. K. Bhaskar, C. T. Nguyen, J. L. Pacheco, H. A. Atikian, C. Meuwly *et al.*, An integrated diamond nanophotonics platform for quantum-optical networks, Science **354**, 847 (2016).
[28] Z. Wang, T. Jaako, P. Kirton, and P. Rabl, Supercorrelated Radiance in Nonlinear Photonic Waveguides, Phys. Rev. Lett. **124**, 213601 (2020).
[29] A. Imamoğlu, H. Schmidt, G. Woods, and M. Deutsch, Strongly Interacting Photons in a Nonlinear Cavity, Phys. Rev. Lett. **79**, 1467 (1997).
[30] I. Carusotto, D. Gerace, H. E. Tureci, S. De Liberato, C. Ciuti, and A. Imamoğlu, Fermionized Photons in an Array of Driven Dissipative Nonlinear Cavities, Phys. Rev. Lett. **103**, 033601 (2009).
[31] C.-E. Bardyn and A. İmamoğlu, Majorana-like Modes of Light in a One-Dimensional Array of Nonlinear Cavities, Phys. Rev. Lett. **109**, 253606 (2012).
[32] G. Kirchmair, B. Vlastakis, Z. Leghtas, S. E. Nigg, H. Paik, E. Ginossar, M. Mirrahimi, L. Frunzio, S. M. Girvin, and R. J. Schoelkopf, Observation of quantum state collapse and revival due to the single-photon Kerr effect, Nature (London) **495**, 205 (2013).
[33] P. Rabl, Photon Blockade Effect in Optomechanical Systems, Phys. Rev. Lett. **107**, 063601 (2011).
[34] A. Nunnenkamp, K. Børkje, and S. M. Girvin, Single-Photon Optomechanics, Phys. Rev. Lett. **107**, 063602 (2011).
[35] K. Stannigel, P. Komar, S. J. M. Habraken, S. D. Bennett, M. D. Lukin, P. Zoller, and P. Rabl, Optomechanical Quantum Information Processing with Photons and Phonons, Phys. Rev. Lett. **109**, 013603 (2012).
[36] X.-W. Xu, Y.-J. Li, and Y.-x. Liu, Photon-induced tunneling in optomechanical systems, Phys. Rev. A **87**, 025803 (2013).
[37] X.-Y. Lü, Y. Wu, J. R. Johansson, H. Jing, J. Zhang, and F. Nori, Squeezed Optomechanics with Phase-Matched Amplification and Dissipation, Phys. Rev. Lett. **114**, 093602 (2015).
[38] S. Mahmoodian, M. Čepulkovskis, S. Das, P. Lodahl, K. Hammerer, and A. S. Sørensen, Strongly Correlated Photon Transport in Waveguide Quantum Electrodynamics with Weakly Coupled Emitters, Phys. Rev. Lett. **121**, 143601 (2018).
[39] D. Tiarks, S. Schmidt-Eberle, T. Stolz, G. Rempe, and S. Dürr, A photon-photon quantum gate based on Rydberg interactions, Nat. Phys. **15**, 124 (2019).
[40] O. A. Iversen and T. Pohl, Strongly Correlated States of Light and Repulsive Photons in Chiral Chains of Three-Level Quantum Emitters, Phys. Rev. Lett. **126**, 083605 (2021).
[41] L. Zhang, V. Walther, K. Mølmer, and T. Pohl, Photon-photon interactions in Rydberg-atom arrays, Quantum **6**, 674 (2022).
[42] S. P. Pedersen, L. Zhang, and T. Pohl, Quantum nonlinear metasurfaces from dual arrays of ultracold atoms, Phys. Rev. Res. **5**, L012047 (2023).
[43] J. E. Sharping, K. F. Lee, M. A. Foster, A. C. Turner, B. S. Schmidt, M. Lipson, A. L. Gaeta, and P. Kumar, Generation of correlated photons in nanoscale silicon waveguides, Opt. Express **14**, 12388 (2006).
[44] C. Xiong, C. Monat, A. S. Clark, C. Grillet, G. D. Marshall, M. Steel, J. Li, L. O'Faolain, T. F. Krauss, J. G. Rarity *et al.*, Slow-light enhanced correlated photon pair generation in a silicon photonic crystal waveguide, Opt. Lett. **36**, 3413 (2011).
[45] Y. Zhang, M. Kues, P. Roztocki, C. Reimer, B. Fischer, B. MacLellan, A. Bisianov, U. Peschel, B. E. Little, S. T. Chu *et al.*, Induced photon correlations through the overlap of two four-wave mixing processes in integrated cavities, Laser Photon. Rev. **14**, 2000128 (2020).
[46] C.-P. Shen, X.-L. Dong, J.-Q. Chen, X.-L. Hei, Y.-F. Qiao, B.-L. Wang, and P.-B. Li, Strong tunable phonon-phonon interactions induced by silicon-vacancy centers in one-dimensional chiral phononic waveguides, Phys. Rev. A **106**, 023717 (2022).
[47] P. Michler, A. Kiraz, C. Becher, W. Schoenfeld, P. Petroff, L. Zhang, E. Hu, and A. Imamoğlu, A quantum dot single-photon turnstile device, Science **290**, 2282 (2000).
[48] H. Wang, Y.-M. He, T.-H. Chung, H. Hu, Y. Yu, S. Chen, X. Ding, M.-C. Chen, J. Qin, X. Yang *et al.*, Towards optimal single-photon sources from polarized microcavities, Nat. Photon. **13**, 770 (2019).
[49] T. C. H. Liew and V. Savona, Single Photons from Coupled Quantum Modes, Phys. Rev. Lett. **104**, 183601 (2010).
[50] M. Bamba, A. Imamoğlu, I. Carusotto, and C. Ciuti, Origin of strong photon antibunching in weakly nonlinear photonic molecules, Phys. Rev. A **83**, 021802(R) (2011).
[51] A. Majumdar, M. Bajcsy, A. Rundquist, and J. Vučković, Loss-Enabled Sub-Poissonian Light Generation in a Bimodal Nanocavity, Phys. Rev. Lett. **108**, 183601 (2012).

[52] Y. H. Zhou, H. Z. Shen, and X. X. Yi, Unconventional photon blockade with second-order nonlinearity, Phys. Rev. A **92**, 023838 (2015).

[53] Y.-L. Liu, G.-Z. Wang, Y.-x. Liu, and F. Nori, Mode coupling and photon antibunching in a bimodal cavity containing a dipole quantum emitter, Phys. Rev. A **93**, 013856 (2016).

[54] Y. H. Zhou, H. Z. Shen, X. Q. Shao, and X. X. Yi, Strong photon antibunching with weak second-order nonlinearity under dissipation and coherent driving, Opt. Express **24**, 17332 (2016).

[55] H. Flayac and V. Savona, Unconventional photon blockade, Phys. Rev. A **96**, 053810 (2017).

[56] B. Sarma and A. K. Sarma, Unconventional photon blockade in three-mode optomechanics, Phys. Rev. A **98**, 013826 (2018).

[57] Y. Yan, Y. Cheng, S. Guan, D. Yu, and Z. Duan, Pulse-regulated single-photon generation via quantum interference in a $\chi^{(2)}$ nonlinear nanocavity, Opt. Lett. **43**, 5086 (2018).

[58] H. Z. Shen, C. Shang, Y. H. Zhou, and X. X. Yi, Unconventional single-photon blockade in non-Markovian systems, Phys. Rev. A **98**, 023856 (2018).

[59] S. Shen, Y. Qu, J. Li, and Y. Wu, Tunable photon statistics in parametrically amplified photonic molecules, Phys. Rev. A **100**, 023814 (2019).

[60] E. Zubizarreta Casalengua, J. C. López Carreño, F. P. Laussy, and E. d. Valle, Conventional and unconventional photon statistics, Laser Photon. Rev. **14**, 1900279 (2020).

[61] H. Jabri and H. Eleuch, Enhanced unconventional photon-blockade effect in one- and two-qubit cavities interacting with nonclassical light, Phys. Rev. A **106**, 023704 (2022).

[62] L. Tian and H. J. Carmichael, Quantum trajectory simulations of two-state behavior in an optical cavity containing one atom, Phys. Rev. A **46**, R6801 (1992).

[63] D.-Y. Wang, C.-H. Bai, X. Han, S. Liu, S. Zhang, and H.-F. Wang, Enhanced photon blockade in an optomechanical system with parametric amplification, Opt. Lett. **45**, 2604 (2020).

[64] M. Chen, J. Tang, L. Tang, H. Wu, and K. Xia, Photon blockade and single-photon generation with multiple quantum emitters, Phys. Rev. Res. **4**, 033083 (2022).

[65] K. M. Birnbaum, A. Boca, R. Miller, A. D. Boozer, T. E. Northup, and H. J. Kimble, Photon blockade in an optical cavity with one trapped atom, Nature (London) **436**, 87 (2005).

[66] C. Lang, D. Bozyigit, C. Eichler, L. Steffen, J. M. Fink, A. A. Abdumalikov, M. Baur, S. Filipp, M. P. da Silva, A. Blais, and A. Wallraff, Observation of Resonant Photon Blockade at Microwave Frequencies Using Correlation Function Measurements, Phys. Rev. Lett. **106**, 243601 (2011).

[67] A. J. Hoffman, S. J. Srinivasan, S. Schmidt, L. Spietz, J. Aumentado, H. E. Türeci, and A. A. Houck, Dispersive Photon Blockade in a Superconducting Circuit, Phys. Rev. Lett. **107**, 053602 (2011).

[68] K. Müller, A. Rundquist, K. A. Fischer, T. Sarmiento, K. G. Lagoudakis, Y. A. Kelaita, C. Sánchez Muñoz, E. del Valle, F. P. Laussy, and J. Vučković, Coherent Generation of Nonclassical Light on Chip via Detuned Photon Blockade, Phys. Rev. Lett. **114**, 233601 (2015).

[69] C. Hamsen, K. N. Tolazzi, T. Wilk, and G. Rempe, Two-Photon Blockade in an Atom-Driven Cavity QED System, Phys. Rev. Lett. **118**, 133604 (2017).

[70] H. J. Snijders, J. A. Frey, J. Norman, H. Flayac, V. Savona, A. C. Gossard, J. E. Bowers, M. P. van Exter, D. Bouwmeester, and W. Löffler, Observation of the Unconventional Photon Blockade, Phys. Rev. Lett. **121**, 043601 (2018).

[71] C. Vaneph, A. Morvan, G. Aiello, M. Féchant, M. Aprili, J. Gabelli, and J. Estève, Observation of the Unconventional Photon Blockade in the Microwave Domain, Phys. Rev. Lett. **121**, 043602 (2018).

[72] R. Huang, A. Miranowicz, J.-Q. Liao, F. Nori, and H. Jing, Nonreciprocal Photon Blockade, Phys. Rev. Lett. **121**, 153601 (2018).

[73] B. Li, R. Huang, X. Xu, A. Miranowicz, and H. Jing, Nonreciprocal unconventional photon blockade in a spinning optomechanical system, Photon. Res. **7**, 630 (2019).

[74] K. Wang, Q. Wu, Y.-F. Yu, and Z.-M. Zhang, Nonreciprocal photon blockade in a two-mode cavity with a second-order nonlinearity, Phys. Rev. A **100**, 053832 (2019).

[75] X. Xu, Y. Zhao, H. Wang, H. Jing, and A. Chen, Quantum nonreciprocality in quadratic optomechanics, Photon. Res. **8**, 143 (2020).

[76] H. Z. Shen, Q. Wang, J. Wang, and X. X. Yi, Nonreciprocal unconventional photon blockade in a driven dissipative cavity with parametric amplification, Phys. Rev. A **101**, 013826 (2020).

[77] W. Xue, H. Shen, and X. Yi, Nonreciprocal conventional photon blockade in driven dissipative atom-cavity, Opt. Lett. **45**, 4424 (2020).

[78] Y.-P. Gao and C. Wang, Hybrid coupling optomechanical assisted nonreciprocal photon blockade, Opt. Express **29**, 25161 (2021).

[79] X. Xia, X. Zhang, J. Xu, H. Li, Z. Fu, and Y. Yang, Giant nonreciprocal unconventional photon blockade with a single atom in an asymmetric cavity, Phys. Rev. A **104**, 063713 (2021).

[80] Y.-W. Jing, H.-Q. Shi, and X.-W. Xu, Nonreciprocal photon blockade and directional amplification in a spinning resonator coupled to a two-level atom, Phys. Rev. A **104**, 033707 (2021).

[81] H. Xie, L.-W. He, X. Shang, G.-W. Lin, and X.-M. Lin, Nonreciprocal photon blockade in cavity optomagnonics, Phys. Rev. A **106**, 053707 (2022).

[82] P. Lodahl, S. Mahmoodian, S. Stobbe, A. Rauschenbeutel, P. Schneeweiss, J. Volz, H. Pichler, and P. Zoller, Chiral quantum optics, Nature (London) **541**, 473 (2017).

[83] S. Maayani, R. Dahan, Y. Kligerman, E. Moses, A. U. Hassan, H. Jing, F. Nori, D. N. Christodoulides, and T. Carmon, Flying couplers above spinning resonators generate irreversible refraction, Nature (London) **558**, 569 (2018).

[84] X.-Y. Yao, H. Ali, F.-L. Li, and P.-B. Li, Nonreciprocal Phonon Blockade in a Spinning Acoustic Ring Cavity Coupled to a Two-Level System, Phys. Rev. Appl. **17**, 054004 (2022).

[85] W. Qin, A. Miranowicz, P.-B. Li, X.-Y. Lü, J. Q. You, and F. Nori, Exponentially Enhanced Light-Matter Interaction, Cooperativities, and Steady-State Entanglement Using Parametric Amplification, Phys. Rev. Lett. **120**, 093601 (2018).

[86] P.-B. Li, Y. Zhou, W.-B. Gao, and F. Nori, Enhancing Spin-Phonon and Spin-Spin Interactions Using Linear Resources in a Hybrid Quantum System, Phys. Rev. Lett. **125**, 153602 (2020).

[87] Y.-H. Chen, W. Qin, X. Wang, A. Miranowicz, and F. Nori, Shortcuts to Adiabaticity for the Quantum Rabi Model:

Efficient Generation of Giant Entangled Cat States via Parametric Amplification, Phys. Rev. Lett. **126**, 023602 (2021).
[88] Y. Wang, J.-L. Wu, J.-X. Han, Y. Xia, Y.-Y. Jiang, and J. Song, Enhanced Phonon Blockade in a Weakly Coupled Hybrid System via Mechanical Parametric Amplification, Phys. Rev. Appl. **17**, 024009 (2022).
[89] X. Guo, C.-L. Zou, H. Jung, and H. X. Tang, On-Chip Strong Coupling and Efficient Frequency Conversion between Telecom and Visible Optical Modes, Phys. Rev. Lett. **117**, 123902 (2016).
[90] J.-Q. Wang, Y.-H. Yang, M. Li, X.-X. Hu, J. B. Surya, X.-B. Xu, C.-H. Dong, G.-C. Guo, H. X. Tang, and C.-L. Zou, Efficient Frequency Conversion in a Degenerate $\chi^{(2)}$ Microresonator, Phys. Rev. Lett. **126**, 133601 (2021).
[91] Z. Ma, J.-Y. Chen, Z. Li, C. Tang, Y. M. Sua, H. Fan, and Y.-P. Huang, Ultrabright Quantum Photon Sources on Chip, Phys. Rev. Lett. **125**, 263602 (2020).
[92] L. Tang, J. Tang, M. Chen, F. Nori, M. Xiao, and K. Xia, Quantum Squeezing Induced Optical Nonreciprocity, Phys. Rev. Lett. **128**, 083604 (2022).
[93] C. Junge, D. O'Shea, J. Volz, and A. Rauschenbeutel, Strong Coupling between Single Atoms and Nontransversal Photons, Phys. Rev. Lett. **110**, 213604 (2013).
[94] M. Scheucher, A. Hilico, E. Will, J. Volz, and A. Rauschenbeutel, Quantum optical circulator controlled by a single chirally coupled atom, Science **354**, 1577 (2016).
[95] C. Sayrin, C. Junge, R. Mitsch, B. Albrecht, D. O'Shea, P. Schneeweiss, J. Volz, and A. Rauschenbeutel, Nanophotonic Optical Isolator Controlled by the Internal State of Cold Atoms, Phys. Rev. X **5**, 041036 (2015).
[96] L. Tang, J. Tang, W. Zhang, G. Lu, H. Zhang, Y. Zhang, K. Xia, and M. Xiao, On-chip chiral single-photon interface: Isolation and unidirectional emission, Phys. Rev. A **99**, 043833 (2019).
[97] H. Eleuch, Photon statistics of light in semiconductor microcavities, J. Phys. B: At. Mol. Opt. Phys. **41**, 055502 (2008).
[98] H. J. Carmichael, R. J. Brecha, and P. R. Rice, Quantum interference and collapse of the wavefunction in cavity QED, Opt. Commun. **82**, 73 (1991).
[99] C. W. Gardiner and M. J. Collett, Input and output in damped quantum systems: Quantum stochastic differential equations and the master equation, Phys. Rev. A **31**, 3761 (1985).
[100] M. Zhang, B. Buscaino, C. Wang, A. Shams-Ansari, C. Reimer, R. Zhu, J. M. Kahn, and M. Lončar, Broadband electro-optic frequency comb generation in a lithium niobate microring resonator, Nature (London) **568**, 373 (2019).
[101] M. Wang, N. Yao, R. Wu, Z. Fang, S. Lv, J. Zhang, J. Lin, W. Fang, and Y. Cheng, Strong nonlinear optics in on-chip coupled lithium niobate microdisk photonic molecules, New J. Phys. **22**, 073030 (2020).
[102] J.-Y. Chen, Z. Li, Z. Ma, C. Tang, H. Fan, Y. M. Sua, and Y.-P. Huang, Photon Conversion and Interaction in a Quasi-Phase-Matched Microresonator, Phys. Rev. Appl. **16**, 064004 (2021).
[103] E. Nitiss, J. Hu, A. Stroganov, and C.-S. Brès, Optically reconfigurable quasi-phase-matching in silicon nitride microresonators, Nat. Photon. **16**, 134 (2022).
[104] R. Wu, J. Zhang, N. Yao, W. Fang, L. Qiao, Z. Chai, J. Lin, and Y. Cheng, Lithium niobate micro-disk resonators of quality factors above 10^7, Opt. Lett. **43**, 4116 (2018).
[105] R. Gao, H. Zhang, F. Bo, W. Fang, Z. Hao, N. Yao, J. Lin, J. Guan, L. Deng, M. Wang *et al.*, Broadband highly efficient nonlinear optical processes in on-chip integrated lithium niobate microdisk resonators of q-factor above 10^8, New J. Phys. **23**, 123027 (2021).
[106] M. Zhang, C. Wang, Y. Hu, A. Shams-Ansari, T. Ren, S. Fan, and M. Lončar, Electronically programmable photonic molecule, Nat. Photon. **13**, 36 (2019).
[107] J. Lu, M. Li, C.-L. Zou, A. Al Sayem, and H. X. Tang, Toward 1% single-photon anharmonicity with periodically poled lithium niobate microring resonators, Optica **7**, 1654 (2020).
[108] Z. Tian, P. Zhang, and X.-W. Chen, Static Hybrid Quantum Nodes: Toward Perfect State Transfer on a Photonic Chip, Phys. Rev. Appl. **15**, 054043 (2021).
[109] T. Kashiwazaki, N. Takanashi, T. Yamashima, T. Kazama, K. Enbutsu, R. Kasahara, T. Umeki, and A. Furusawa, Continuous-wave 6-dB-squeezed light with 2.5-THz-bandwidth from single-mode PPLN waveguide, APL Photon. **5**, 036104 (2020).
[110] V. D. Vaidya, B. Morrison, L. Helt, R. Shahrokshahi, D. Mahler, M. Collins, K. Tan, J. Lavoie, A. Repingon, M. Menotti *et al.*, Broadband quadrature-squeezed vacuum and nonclassical photon number correlations from a nanophotonic device, Sci. Adv. **6**, eaba9186 (2020).
[111] Y.-C. Liu, X. Luan, H.-K. Li, Q. Gong, C. W. Wong, and Y.-F. Xiao, Coherent Polariton Dynamics in Coupled Highly Dissipative Cavities, Phys. Rev. Lett. **112**, 213602 (2014).
[112] L. R. Bakker, M. S. Bahovadinov, D. V. Kurlov, V. Gritsev, A. K. Fedorov, and D. O. Krimer, Driven-Dissipative Time Crystalline Phases in a Two-Mode Bosonic System with Kerr Nonlinearity, Phys. Rev. Lett. **129**, 250401 (2022).
[113] J. R. Johansson, P. D. Nation, and F. Nori, QuTiP: An open-source Python framework for the dynamics of open quantum systems, Comput. Phys. Commun. **183**, 1760 (2012).